CFD MODELLING OF WIND TURBINE AIRFOIL AERODYNAMICS

63° CONGRESSO NAZIONALE ATI
ASSOCIAZIONE TERMOTECNICA ITALIANA

M.S. Campobasso[1], A. Zanon[2], M. Foerster[3], F. Fraysse[4], A. Bonfiglioli[5]

[1]Department of Aerospace Engineering, University of Glasgow, G12 8QQ Glasgow, United Kingdom,
, [2]Dipartimento di Energetica e Macchine, Universita' di Udine, 33100 Udine, Italy
[3]Lehrstuhl für Fluidmechanik, Technische Universität München, D-85748 Garching, Germany
[4]Ecole Nationale Supérieure de Mécanique et d'Aérotechnique, 86360 Poitiers, France
[5]Dipartimento di Ingegneria e Fisica dell'Ambiente, Universita' della Basilicata, 85100 Potenza, Italy

SUMMARY

This paper reports the first findings of an ongoing research programme on wind turbine computational aerodynamics at the University of Glasgow. Several modeling aspects of wind turbine airfoil aerodynamics based on the solution of the Reynolds-averaged Navier-Stokes (RANS) equations are addressed.

One of these is the effect of an *a priori* method for structured grid adaptation aimed at improving the wake resolution. Presented results emphasize that the proposed adaptation strategy greatly improves the wake resolution in the far-field, whereas the wake is completely diffused by the non-adapted grid with the same number and distribution of grid nodes. A grid refinement analysis carried out with the adapted grid shows that the improvements of flow resolution thus achieved are of a smaller magnitude with respect to those accomplished by adapting the grid keeping constant the number of nodes. The proposed adaptation approach can be easily included in the structured generation process of both commercial and in-house structured mesh generators systems.

The study also aims at quantifying the solution inaccuracy arising from not modeling the laminar-to-turbulent transition. It is found that the drag forces obtained by considering the flow as transitional or fully turbulent may differ by 50 %.

The impact of various turbulence models on the predicted aerodynamic forces is also analyzed.

All these issues are investigated using a special-purpose hyperbolic grid generator and a multi-block structured finite-volume RANS code. The numerical experiments consider the flow field past a wind turbine airfoil for which an exhaustive campaign of steady and unsteady experimental measurements was conducted. The predictive capabilities of the CFD solver are validated by comparing experimental data and numerical predictions for selected flow regimes. The incompressible analysis and design code XFOIL is also used to support the findings of the comparative analysis of numerical RANS-based results and experimental data.

INTRODUCTION

Improving the steady and unsteady aerodynamic performance of existing Wind Turbines (WT's) and designing the next generation of more powerful and more reliable machines will increasingly require the use of high-fidelity aerodynamic models such as those of Computational Fluid Dynamics (CFD), and also a substantial level of confidence in the potential of this technology.

Outstanding studies on the current capabilities of Computational Fluid Dynamics (CFD) to predict the steady and unsteady aerodynamics of WT airfoils have appeared in the past few years (see articles [1,2,3]), but the level of public domain knowledge and experience in this area is still significantly lower than in related fields, such as aircraft wing or turbomachinery blade computational aerodynamics.

One of the crucial phases in the design of new WT blades is the accurate prediction of the aerodynamic forces and the flow field past the airfoils making up their outer shape. The radial integral of such forces determines both the overall torque (and thus the power) available at the shaft, and the axial thrust acting on the turbine, which is needed to size the support of the tower.

The use of CFD codes solving the Reynolds-averaged Navier-Stokes (RANS) equations is emerging as a viable option to accomplish this objective. However, their employment in WT aerodynamics presents several important challenges. Some of these arise because the flow field past the blade is transitional over the whole blade height. Indeed, the Reynolds number decreases dramatically from tip to hub, and the highest value occurring at the tip is already in the transitional regime. The Mach number also varies substantially along the blade, being always in the low subsonic range and achieving extremely low levels at the hub. These features point to the necessity of suitably accounting for laminar-to-turbulent transition and incompressibility effects. Among the studies on the issue of transition, remarkable studies are those of the articles [4] and [5], whereas a striking example of the low Mach number effects on the prediction of separated airfoil flows is reported in [3]. An additional factor which may affect the CFD prediction of airfoil forces is the choice of the turbulence models. The results of [3], for example, show that the prediction of the flow field past a WT airfoil with an incidence of 12^o does not reveal any flow separation when using the $K-\omega$ turbulence model reported in the article [6], whereas a heavily stalled flow field is obtained when using the Shear Stress Transport (SST) $K-\omega$ model described in the article [7].

The aforementioned turbulence-model-related modeling issues are particularly crucial if the forces acting on the airfoil are to be determined by means of the so-called *near field*

method, whereby lift, drag and moment are determined by means of surface integration of local pressure and frictional forces. Prompted by some mistrust in the turbulence model prediction of the wall viscous stress and also by the necessity of very high grid refinement near viscous walls, however, a *mid-field* approach for the calculation of the airfoil forces has recently received some attention [8]. Starting from a given RANS solution, this method determines the airfoil forces by using the velocity field in the boundary layers and the wake. Reported results show that the drag computed with the mid-field approach is much less sensitive to the refinement on viscous walls than the near-wall integration method. The former technique, however, assumes a sufficient wake resolution.

When using structured CFD codes, however, special care has to be taken when meshing the wake region of the C-grid, typically used for the aerodynamic analysis of airfoils with a sharp Trailing Edge (TE). This is because the geometry of several families of WT airfoils consists of a non-symmetric profile with a sharp and cambered TE, and these features result in a locally concave shape of the lower side. In this circumstance, the use of a standard C-grid with a straight cut may introduce unacceptable under-resolution of the wake, making questionable the use of mid-field methods. This problem can be solved by a) increasing the refinement in the wake region, b) by adapting the geometry of the grid in the wake region to the wake or c) by a combination of both actions.

The primary objective of this paper is to present an *a priori* mesh adaptation method aimed at improving the wake resolution of a given C-mesh used for the CFD analysis of WT airfoils. The technique does only vary the local mesh geometry, and does not alter the overall number of grid nodes. This modeling flexibility is also used to quantify the impact that a varying wake resolution may have on the aerodynamic forces computed with the standard near-field method. The effect of the grid refinement on the forces using the adapted and standard (i.e. straight- and horizontal-cut) grid is also assessed.

The second thread of the paper is the analysis of the effect of turbulence modeling on the predicted flow field and airfoil characteristics. To this aim, a comparative analysis based on the use of several turbulence models in the RANS CFD code is also presented.

All presented investigations are based on simulations and measurements of the flow field past the FFA-W3-241 WT airfoil provided in the report [9], which is depicted in Figure 1. The numerical simulations have been carried out by means of a structured finite-volume RANS code featuring several different turbulence models, and the incompressible analysis and design code XFOIL which uses a coupled potential flow and integral boundary layer model and a very accurate transition model. The predictive capabilities of the RANS code are assessed by comparing its predictions to the experimental data and the XFOIL results.

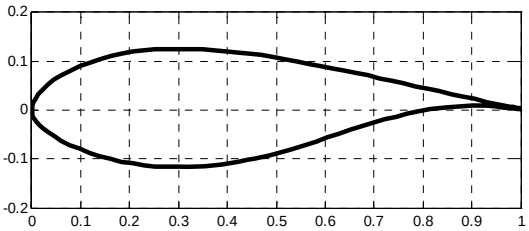

Figure 1 Profile of FFA-W3-241 airfoil.

GRID GENERATION

The grids adopted in this study have been generated by the structured grid generator WINGRID described in the technical reports [10] and [11]. The code builds a C-grid past the airfoil by solving a system of two hyperbolic partial differential equations with an implicit discretization. The grids are orthogonal, and the generation process allows a high degree of control of node stretching and local distance from all boundaries. One of the original features of WINGRID is the possibility of actively controlling the geometry of the C-cut. Three options are available: *a)* straight horizontal cut, *b)* straight cut rotated by a user-given angle, and *c)* coordinates of grid-cut geometry provided by the user. As shown in the result sections, the grid constructed using the third option yields the best resolution of the flow field past airfoils with sharp and cambered TE. This is because the wake shed by these airfoils has a fairly complex trajectory: soon after the TE, the flow is aligned with the airfoil camber line, and then it takes the freestream direction within one chord length from the TE. The first patch of this pattern is highlighted in Figure 2, the three sketches of which depict the C-cut obtained using the three aforementioned options and the TE streamline computed by the RANS-based CFD code for a freestream direction $\alpha=4^{o}$.

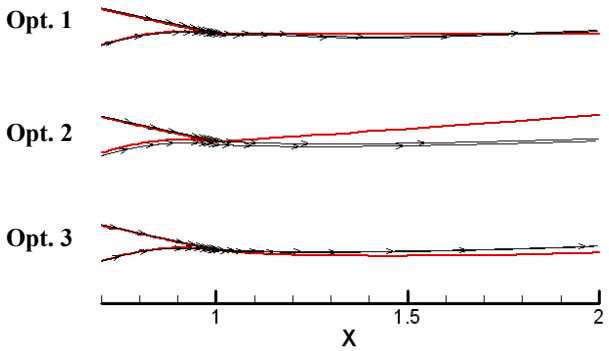

Figure 2 Geometry option for C-cut construction

As expected, the straight horizontal cut of option 1 is intersected by the wake, directed downwards at the TE and upwards from about 40 % chord lengths to the exit of the computational domain; the straight cut of option 2 rotated by α completely misses the wake because the direction of the C-cut and the wake close to the TE are initially opposite. The user-given cut geometry of option 3 is that which best tracks the wake. The importance of aligning the C-cut and the wake relies in that the maximum grid refinement in the normal direction is concentrated around the cut, and therefore the wake/cut alignment guarantees the best wake resolution.

The misalignment of C-cut and wake has potentially negative consequences also further downstream, as illustrated in Figure 3-a and Figure 3-b. The plots report the farfield grid obtained by using options 1 and 3 respectively, and these grids are generated for the CFD analysis of the flow field with a freestream direction of 10.2^{o}. The computed streamline is also reported in both figures. One sees how the wake rapidly moves to a region with scarce grid refinement in the case of the straight horizontal cut (Figure 3-a). Conversely Figure 3-b shows that the computed wake remains in a high-refinement region even in the farfield region, though not exactly in the middle of the maximum refinement band about the C-cut. The

wake also appears not to be parallel to the C-cut. This is due to a slight mismatch between the wake computed by CFD and the user-given geometry of the cut. Further downstream, the computed wake and the C-cut become parallel as shown in Figure 4.

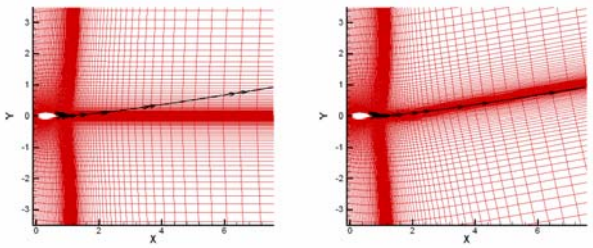

a) b)

Figure 3 Enlarged view of C-grid behind airfoil: a) straight horizontal C-cut, and b) adapted C-cut.

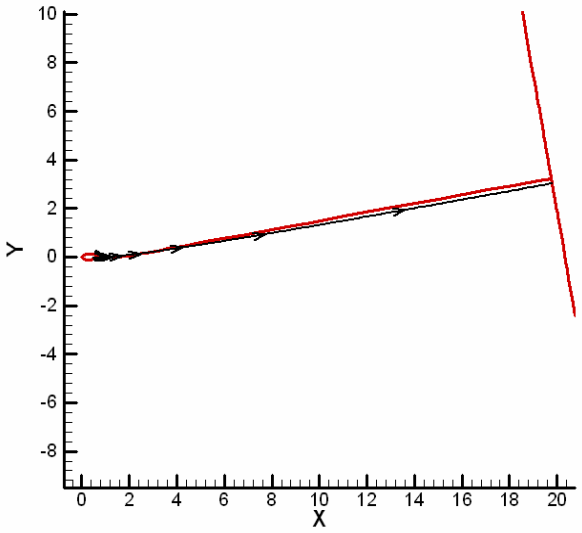

Figure 4 Wake trajectory and C-cut of wake-adapted grid.

The user-given cut profile is generated as follows: for the first chord length behind the TE one uses the streamline predicted by XFOIL for the given freestream direction; a straight line rotated by α is instead used from the end of the XFOIL streamline to the downstream farfield boundary of the C-grid. Since this construction of the C-cut is based on a forecast of the wake trajectory, we call this process an *a priori* grid adaptation method. Note that the CPU-time of a single XFOIL analysis amounts to fractions of a second, making this cost negligible with respect to that required for the grid generation.

The CFD results presented in this paper will highlight the substantial differences of flow resolution and convergence property of the CFD solver achieved by using the adaptive geometry of the cut. It should be noted that the importance of aligning the wake grid with the mid- and far-field wake had been already recognized, as shown by the multi-block grids used in the article [12]. The importance of the following results, however, is to emphasize the necessity of adapting the wake grid also in the TE proximity.

CFD CODE

The RANS CFD code used for all flow simulations reported in this paper is ISAAC, a structured multi-block solver based on a second order upwind finite-volume space-discretization. Advection terms in the mean flow and turbulence equations are solved using Roe's approximate Riemann solver coupled with MUSCL extrapolations, whereas viscous terms are calculated with a central difference approximation. Mean flow and turbulence equations are solved in a coupled fashion using an implicit spatially split diagonalized approximate factorization. The multigrid algorithm is also made use of to speed up convergence. The interested reader is referred to the article [13] for further details on the algorithmic aspects of ISAAC.

This solver features several turbulence closure models, including the K-ω model [6], the variant of the K-ε model described in the article [14], and an Algebraic Stress Model (ASM) versions of both K-ω and the K-ε models [15]. The turbulence models reported in [14] and [6] use linear relationship between the Reynolds stress and the strain rate tensors (Boussinesq approximation), whereas the ASM counterpart of both models uses nonlinear algebraic relationships between the component of the Reynolds stress tensor and those of the velocity gradient. The impact of these models on the computed flow field past the FFA-W3-241 airfoil is assessed in the following result sections. Note that all four models are low-Reynolds-number models, and they can thus be integrated down to viscous walls without requiring wall functions.

EFFECTS OF GRID ADAPTATION, GRID REFINEMENT AND TRANSITION MODELING ON COMPUTED FLOW FIELD

Experimental measurements of the flow field past the FFA-W3-241 airfoil have been performed for a freestream Mach number of 0.11 and a Reynolds number of 1.6×10^6, and for several values of freestream incidences. Steady and unsteady flow regimes have been analyzed, and this section considers the two steady regimes associated with an incidence of 4.02^o and 10.2^o. The CFD simulations reported in this section use the low Reynolds number K-ε ASM model.

Effect of adaptation and transition modeling, α=4.02°

Preliminary mesh sensitivity and refinement analysis have led to the choice of a C-grid with the following features: number of nodes past the airfoil I_{bb}=301, minimum distance from airfoil surface in chord units dn=5x10^{-7}, number of nodes in the normal direction j_{max}=129, and number of nodes in C-cut I_{bc}=81. The overall number of points on the C-lines is thus I_{max}=461, and this grid, which we call *level 1*, has an overall number of points of N_{node}=59469. The farfield boundary is at about 20 chords from the airfoil in all directions. The level 1 grid has been generated in two versions: one featuring a straight horizontal C-cut (option 1), and the other featuring a user-given cut geometry (option 3) based on an XFOIL analysis for the given Reynolds and Mach numbers and $\alpha = 4.02°$. These two meshes have the same number of nodes. The topological difference between these grids is the same as that between those of Figure 3.

The CFD flow analysis based on the K-ε ASM model for $\alpha = 4.02°$ has led to a maximum y^+ of 0.54 using either grid

topology. This highlights that the selected wall distance is adequate for resolving the airfoil boundary layers. The contours of total pressure obtained by using the standard and adapted grids are reported in Figure 5. The definition of the total pressure coefficient is:

$$C_{p^0} = \frac{p_{0,\infty} - p_0}{q_\infty}$$

where $p_{0,\infty}$ and p_0 denote freestream and local total pressure respectively, and q_∞ is the freestream dynamic head.

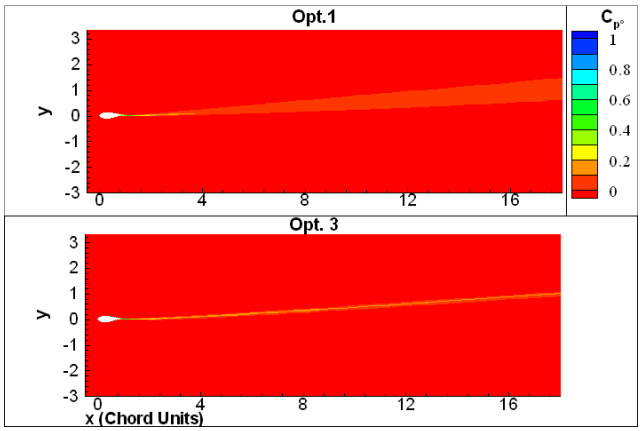

Figure 5 Contours of total pressure coefficients computed with standard grid (option 1) and wake adapted grid (option 3) for α=4.02°.

The results of Figure 5 show that the wake resolution of the CFD simulation with adapted grid (option 3) has substantially improved with respect to that of the standard grid (option 1). In the former case, in fact, the wake is significantly sharper and less diffused. This effect is quantified in Figure 6, which reports the total pressure coefficient at 1, 3, 5, 7, 9 and 11 chord lengths after the TE. This sequence shows that the solution of the grid with straight horizontal cut has already a very diffused (shallow) trace of the wake at 7 chords from the TE, whereas the solution of the adapted grid still features a physically much more likely sharp wake at 11 chord lengths behind the TE.

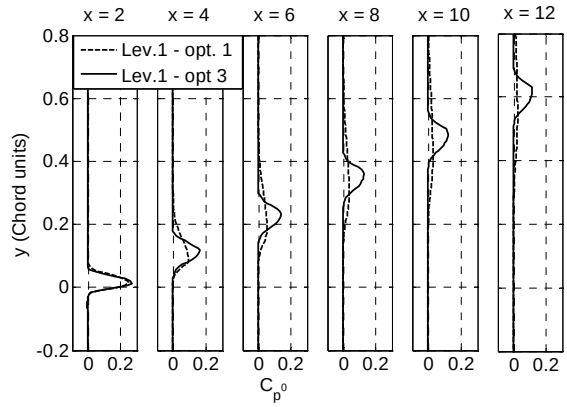

Figure 6 Comparative analysis of wake evolution computed with standard and wake-adapted grid for α=4.02°.

The alignment of the wake and the C-cut also has a strong impact on the convergence rate of the CFD analysis. The four subplots of Figure 7 present the convergence history of the continuity, x- and y-component of the momentum and energy equations obtained by using the grid with straight horizontal cut (option 1), that with straight rotated cut (option 2) and with wake-adapted cut (option 3). One sees that the worst convergence rate is obtained with the option 1 grid. In this case, the maximum flow residuals occur in the wake shortly after the TE in the area where the wake leaves the high refinement area past the C-cut. A better convergence rate is obtained with the rotated cut (option 2), but the best rate is achieved with the wake-adapted grid. These observations highlight that the adopted adaptation strategy not only improves the resolution of the flow field, but also improves the convergence properties of the CFD solver.

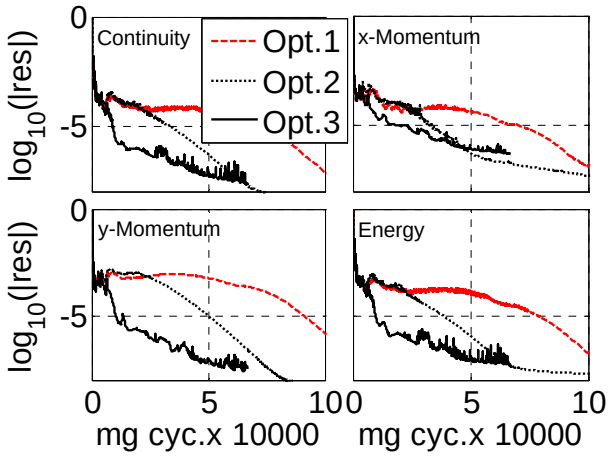

Figure 7 Converge histories of CFD solver with option 1, option 2 and option 3 grid for α=4.02°.

The ISAAC CFD code also allows to enforce the streamwise position where the laminar-to-turbulent transition occurs. This feature has been exploited in the present analyses. The chordwise position of the transition on both airfoil sides has been determined by the same XFOIL analysis used to determine the cut geometry for WINGRID. These transition positions have been used as input for the ISAAC analyses. Figure 8 provides the skin friction coefficient on the airfoil surface predicted by the two transitional RANS calculations (results labeled trns.') and by XFOIL. These data highlight a good agreement between the results of the two codes. Note also that the two transitional RANS profiles present negligible differences. This seems to indicate that the extent to which we resolve the wake has negligible impact on the prediction of the drag computed by surface integration of the viscous stress. It should be noted, however, that this conclusion will most likely not hold for flow fields which, unlikely that considered here, have a significant level of flow unsteadiness Figure 8 also shows that both ISAAC transitional profiles and the XFOIL profile show a sudden rise of C_f at about 35 % chord on the upper side and about 45 % on the lower side. These are the positions at which transition occurs. The sharp increment of viscous tress is caused by the fact that the wall viscous stress in the turbulent boundary layer is higher than in the laminar boundary layer preceding the transition. Figure 8 also reports the profile obtained with a fully turbulent RANS analysis (result labeled 'turb.'). This analysis overpredicts the drag force, due to the substantially higher level of C_f that it attributes to the the front part of the airfoil boundary layers. This significant difference between fully turbulent and transitional profiles emphasizes the importance of modeling transition when using CFD for WT design.

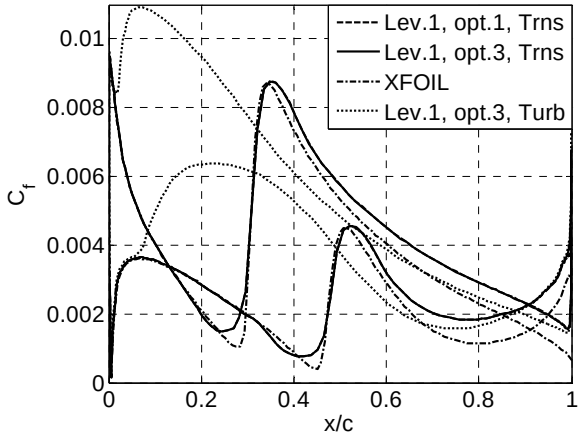

Figure 8 Computed profiles of skin friction coefficient $\alpha=4.02^o$.

Computed and measured profiles of static pressure coefficient C_p are presented in Figure 9. The definition of this parameter is:

$$C_p = \frac{p - p_\infty}{q_\infty}$$

where p_∞ and p_0 denote freestream and local static pressure respectively. Similarly to the case of the skin friction coefficient, one sees that a) there are no visible differences between the transitional RANS results obtained with the standard and adapted grid, b) these two transitional CFD results and the XFOIL prediction are in excellent agreement, and c) the CFD profile obtained with a fully turbulent analysis deviates from all transitional numerical results in the first 35% of the upper side, where transitional analyses place the transition. The difference between transitional and fully turbulent profiles on the lower side is very small. As for the comparison between measured and computed data, some differences between all computed transitional results and the experimental data are visible in the front and rear part of the upper side. The fact that the RANS-based and XFOIL profiles present negligible differences despite the fact that they use substantially different flow models, makes it possible to assume that some wind tunnel effects may be responsible for the aforementioned differences.

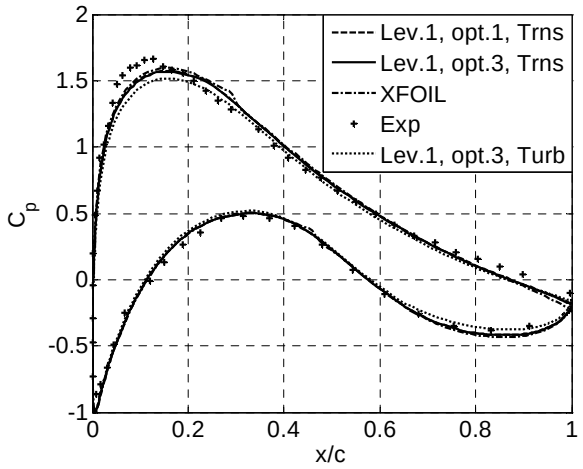

Figure 9 Computed and measured profiles of static pressure coefficient $\alpha=4.02^o$.

As reported in [9], measurements of the total pressure in the wake were also made. A fixed vertical rake of pressure taps was positioned behind the airfoil. The variation of the flow incidence was enabled by rotating the airfoil about a hinge placed at 40 % of its chord. The distance between the TE and the wake rake of the airfoil was 70 % chord lengths when the airfoil was in the horizontal position. The measured profile of total pressure coefficient in the wake and that computed by the wake-adapted RANS analysis are compared in Figure 10. The overall agreement between depth and width of computed and measured profiles is fairly good. The centerline of the computed profile appears to have a left offset with respect to the measured profile. Conversely, the position of the TE streamline predicted by XFOIL is closer to the centerline of the measured wake. This comparison is affected by some uncertainty, such as the effects of top and bottom tunnel walls on the streamline trajectory. As reported in [9], these latter are not taken into account in the experimental corrections.

The effect of the grid adaptation on the wake resolution for $\alpha=4.02^o$ is not significant within one chord length from the TE (see Figure 6). Hence the profile computed with the option 1 grid does not differ from the computed profile in Figure 10.

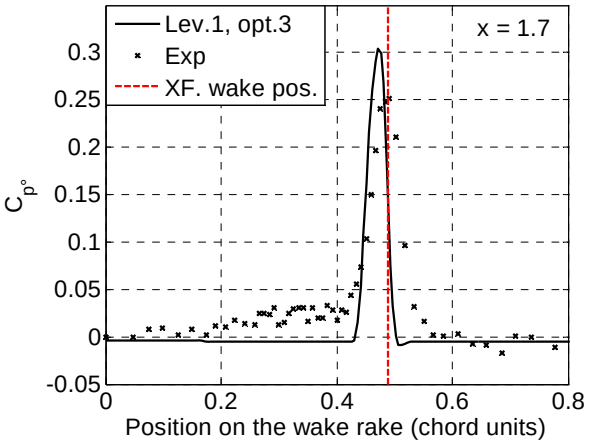

Figure 10 Measured and computed profiles of total pressure coefficient behind the airfoil TE for $\alpha=4.02^o$.

The numerical and experimental values of lift coefficient C_L and drag coefficient C_D are reported in Table 1. All numerical values are obtained by integrating pressure force and viscous stress on the airfoil surface. The experimental estimate of the forces is instead obtained by integrating the measured static pressure distribution on the airfoil, and applying a momentum balance approach to a control volume enclosing the airfoil. The momentum balance calculation makes use of the wake rake data. Further detailed on the calculation of the forces are provided in [9]. The first two columns of Table 1 report C_L and C_D computed by transitional RANS analyses with the standard and adapted grid respectively; the third row has the force coefficients computed by a fully turbulent RANS analysis with adapted grid, and the last two columns have the XFOIL and experimental estimates, respectively. One notices that: 1) the mesh adaptation in the wake region has a negligible effect on the drag force, and a small effect (variation of about 0.5 %) on the lift force; 2) the error induced by not accounting for laminar-to-turbulent transition is about 7 % for the lift and 50 % for the drag; 3) lift and drag predicted by the transitional CFD analyses are in reasonably good agreement with experimental data, and the level of agreement is of the same order as that between XFOIL and the experimental data.

Table 1 Measured and computed force coefficients (level 1 grid for CFD analyses) for $\alpha=4.02^o$.

	L1 - 01 Trns	L1 - 03 Trns	L1 - 03 Turb	XFOIL	Exp
Cl	0.7578	0.75306	0.70052	0.7691	0.769
Cd	0.011541	0.011509	0.016871	0.00928	0.0126

Effect of adaptation, $\alpha=10.2^o$

The level 1 grid has been considered again in the two versions, with straight horizontal C-cut (option 1), and with the user-given cut geometry (option 3) based on an XFOIL analysis for $\alpha=10.2^o$. Note that the former grid is identical to its counterpart for the case of $\alpha=4.02^o$.The CFD flow analysis based on the K-ε ASM model for $\alpha=10.2^o$ has led to a maximum y^+ of 0.71 using either grid topology.

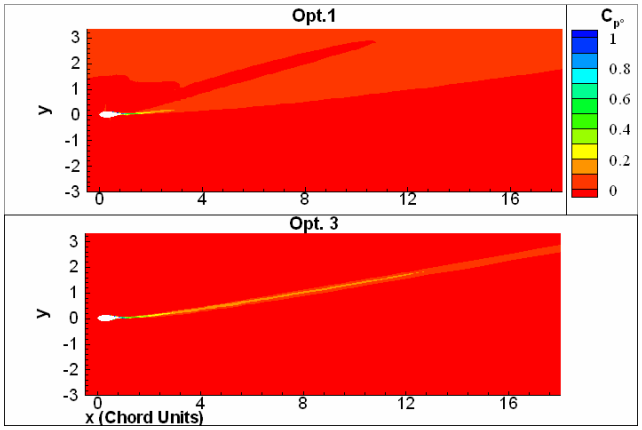

Figure 11 Contours of total pressure coefficients computed with standard grid (option 1) and wake adapted grid (option 3) for $\alpha=10.2^o$.

The contours of total pressure obtained by using the standard and adapted grids are reported in Figure 11. These results show that the improvement of the wake resolution achieved by using the wake-adapted grid is even bigger than for the case $\alpha=4.02^o$. Figure 12 reports the comparative evolution of C_p^o in the wake. It highlights that the wake diffuses even faster than in the $\alpha=4.02^o$ case, and it also highlights that the effects of insufficient grid resolution are now felt also before one chord length from the TE.

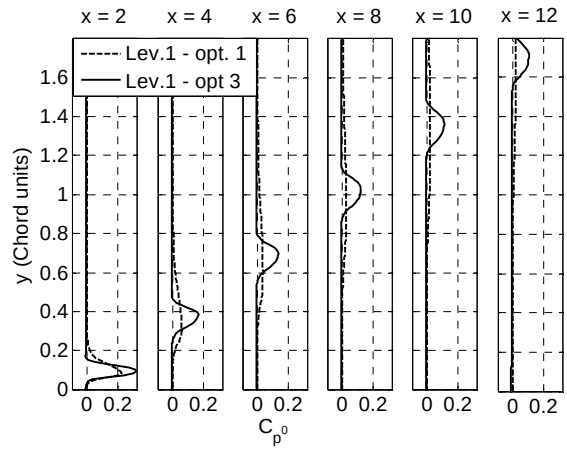

Figure 12 Comparative analysis of wake evolution computed with standard and wake-adapted grid for $\alpha=10.2^o$.

The effect of the wake/cut misalignment on the convergence of the CFD solver for this incidence is analyzed in Figure 13, which reports the convergence history of the continuity, x- and y-component of the momentum and energy equations obtained by using the standard and the adapted grids. The worst convergence rate is obtained again with the straight-horizontal-cut grid. Also for this incidence, the maximum residuals occur in the wake shortly after the TE in the area where the wake leaves the high refinement area past the C-cut.

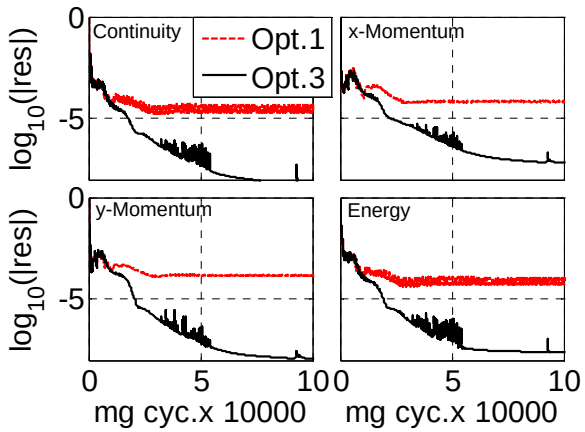

Figure 13 Converge histories of CFD solver with option 1, option 2 and option 3 grid for $\alpha=10.2^o$.

Figure 14 provides the skin friction coefficient on the airfoil surface predicted by the two RANS calculations using the option 1 and option 3 grids. Both results refer to transitional computations, and the positions of the transition have been taken to be those predicted by XFOIL, the profile of which is also reported. These plot shows that there is an excellent agreement between XFOIL and ISAAC as long as the boundary layer remains laminar, After transition, however, the evolution of the turbulent viscous layers predicted by the two codes present some relevant differences, particularly on the upper side of the airfoil. Similarly to the 4.02° incidence case, however, the wake-driven adaptation appears to have no effect on the wall stress predicted by the CFD code.

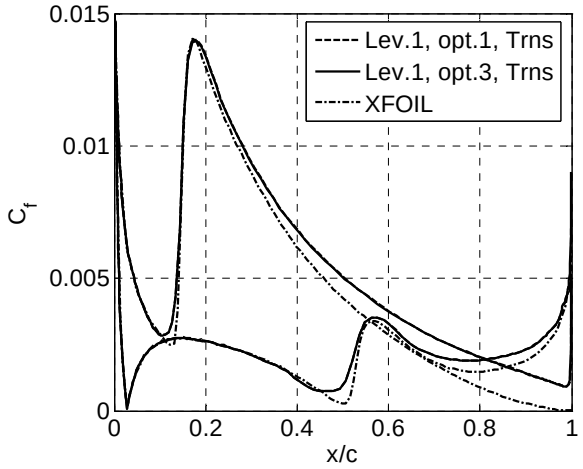

Figure 14 Computed profiles of skin friction coefficient $\alpha=10.2^o$.

Computed and measured profiles of static pressure coefficient

C_p are presented in Figure 15. The conclusions drawn by the analysis of these profiles are the same as those for the 4.02° incidence flow, namely a) there are no visible differences between the transitional RANS results obtained with the standard and adapted grid, and b) these two transitional CFD results and the XFOIL prediction are in excellent agreement, and as for the comparison between measured and computed data, some differences between all computed transitional results and the experimental data are visible from 10 to 60 % chord on the upper side. Such differences may be possibly due to some wind tunnel effects, such as the influence of top and bottom walls on streamline curvature.

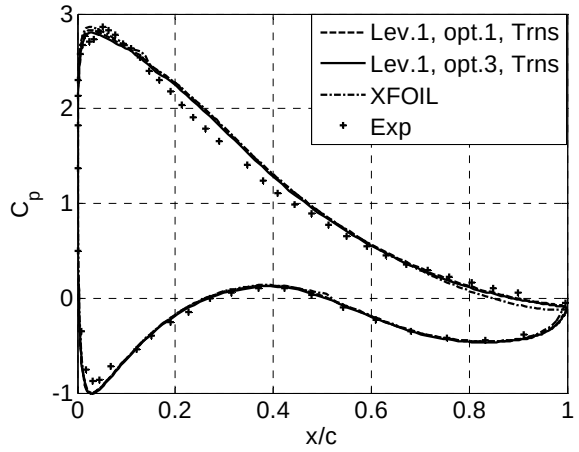

Figure 15 Computed and measured profiles of static pressure coefficient *α=10.2°*.

Measured and computed total pressure coefficient at 70 % chord length after the TE are plotted in Figure 16. As the wake-adaptivity has an effect on the wake resolution also closer to the TE than in the 4.02° incidence case, both standard and wake-adapted CFD results are reported. It is observed that total pressure deficit predicted by the adapted grid is slightly higher than with the option 1 grid. Width and depth of both CFD analyses, however, are comparable and fairly similar to those of the measurements. As for the other incidence, the CFD-based centerline of the wake has a left offset with respect to that of the measured profile, whereas the position of the XFOIL TE streamline seems to better match the experimental data.

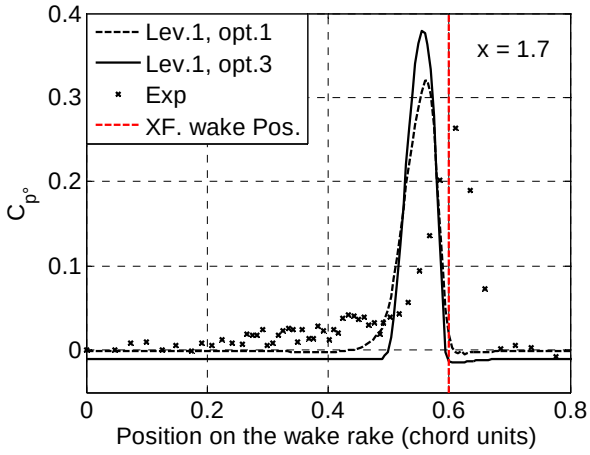

Figure 16 Measured and computed profiles of total pressure coefficient behind the airfoil TE for *α=10.2°*.

The computed and measured force coefficients for *α=10.2°* are reported in Table 2. These numbers reveal a comparable level of agreement between RANS and measured data, and also between XFOIL and measured data. The overall agreement of both types of numerical simulations and experimental data, however, is slightly worse than for *α=4.02°*.

Table 2 Measured and computed force coefficients (level 1 grid for CFD analyses) for *α=10.2°*.

	L1 - 01 Trns	L1 - 03 Trns	XFOIL	Exp
C_L	1.4016	1.3949	1.3884	1.344
C_D	0.02038	0.02042	0.01548	0.0171

EFFECTS OF TURBULENCE MODELING ON COMPUTED FLOW FIELD

In order to assess the influence of turbulence modeling on the computed forces, the flow field past the FFA=W3-241 airfoil for *α=10.2°* has been computed using also the *K-ω* model, and the ASM version of both the *K-ω* and the *K-ε* models. The skin friction coefficient computed with all four models is plotted in Figure 17. Overall the best agreement between XFOIL and ISAAC is obtained with the *K-ω* ASM model. On the upper side, some deviations between these two results are only observed from 70 % chord to the TE.

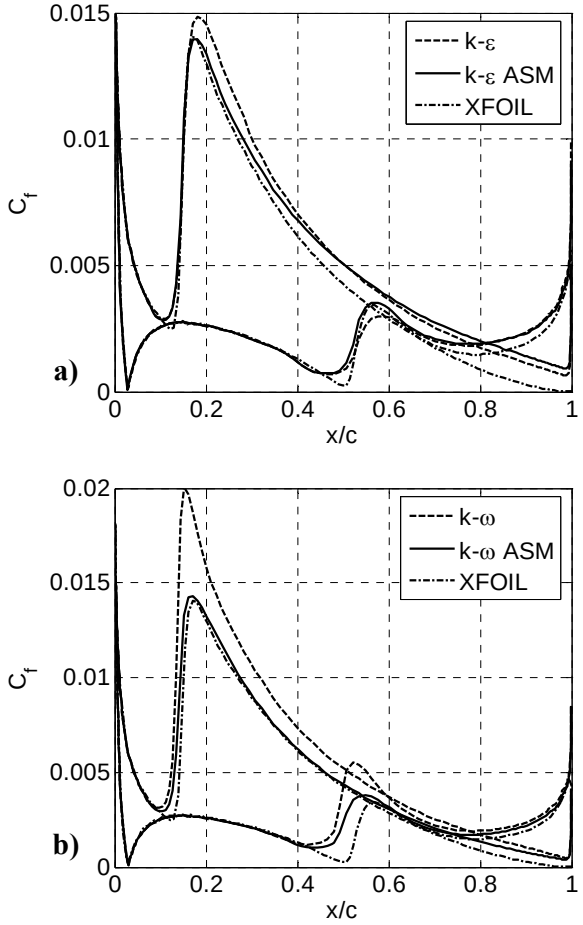

Figure 17 Comparative analysis of turbulence models for *α=10.2°*: a) skin friction coefficient computed with *K-ε* and *K-ε* ASM models, and b)skin friction coefficient computed with *K-ω* and *K-ω* ASM

models.

At present, it is not clear why both *K-ω* appear not to trigger the laminar-to-turbulent transition at the same positions of XFOIL. These latter have been prescribed as input for all four calculations, but only the two *K-ε* analyses appear to place the transition exactly where required.

Figure 18 depicts the static pressure coefficient determined by all four CFD analyses and XFOIL, and shows that the differences among all results are negligible.

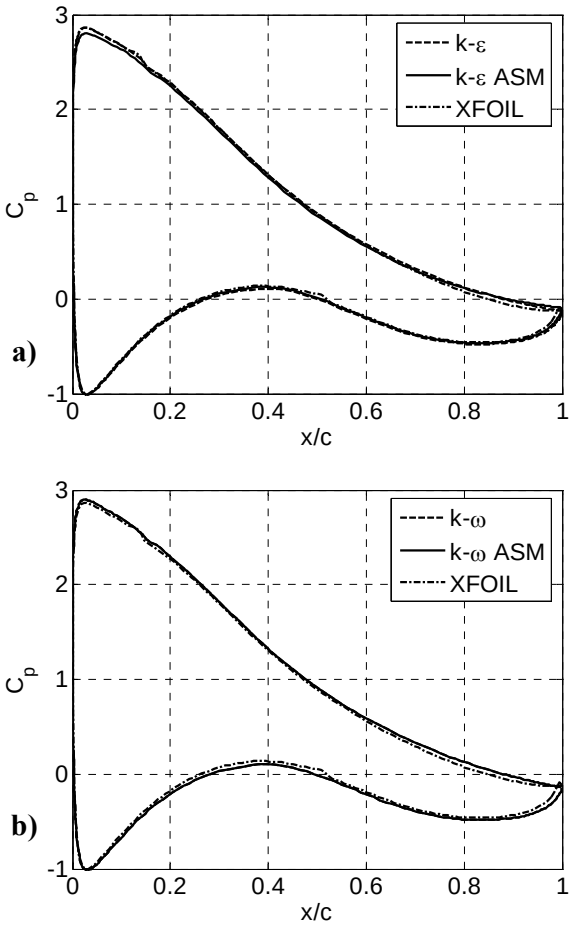

Figure 18 Comparative analysis of turbulence models for *α=10.2°*: a) skin friction coefficient computed with *K-ε* and *K-ε* ASM models, and b) skin friction coefficient computed with *K-ω* and *K-ω* ASM models.

The total pressure deficit in the wake computed by using the four turbulence models is compared to the wake rake data in Figure 19-a and Figure 19-b. The most remarkable difference between the *K-ε* and *K-ω* models, are that 1) the former ones predict a minimum total pressure in the wake which is about 25 % lower than the predictions of the latter models, and 2) the width of the wake predicted by the *K-ω* models is slightly larger than the width computed by the other two models. Both features appear to make the prediction of the *K-ω* models closer to the experimental data. On the other hand, the use of either the linear eddy viscosity model associated with Boussinesq approximation or the ASM expression of the Reynolds stress tensor seems to make little difference for both *K-ε* and *K-ω* models. This is highlighted by the fact that there are small differences between the two profiles of Figure 19-a, and also between those of Figure 19-b.

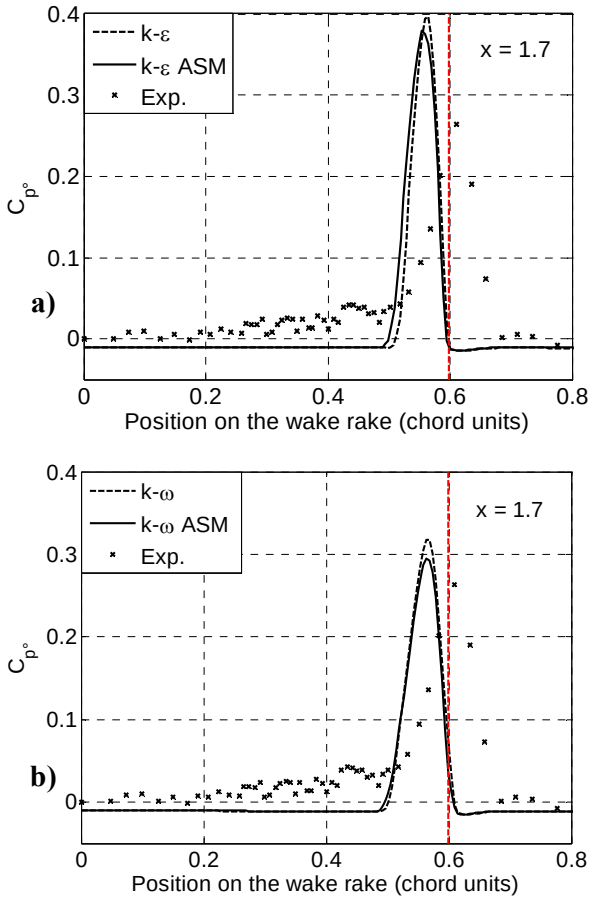

Figure 19 Comparative analysis of total pressure coefficient at 70% chord from TE using different turbulence models for *α=10.2°*: a) profiles computed by *K-ε* and *K-ε* ASM models, and b) profiles computed by *K-ω* and *K-ω* ASM models.

Finally, the computed force coefficients using the four models are reported in Table 3. The best prediction of the lift force seems to be that of the *K-ε* ASM model, whereas the best drag prediction appear to be that of the *K-ω* ASM model. It should be observed that the experimental values of lift and drag coefficients have been obtained using different methods (lift by airfoil pressure integration, and drag by using wake rake data for momentum balance). Hence it is possible that the two experimental forces may be affected by different types and level of uncertainties, which probably explains why the best prediction of lift and drag appear to be given by two different analyses.

Table 3 Computed force coefficients (level 1 grid) for *α=10.2°* using 4 different turbulence models.

	k - ε	k - ε ASM	k - ω	k - ω ASM	Exp
Cl	1.43	1.3949	1.4633	1.4495	1.344
Cd	0.01927	0.020426	0.019728	0.01839	0.0171

EFFECT OF GRID REFINEMENT

In this section, we keep the grid topology of the adapted grid and we examine the effect of grid refinements on the wake resolution. Three additional grid levels (2 to 4) have

been considered, with the level of grid refinement increasing from level 1 to level 4. As this study focuses primarily on the effects of adaptation and refinement in the wake region, all four grids have the same number of nodes past the airfoil and the same minimum normal distance at the airfoil wall boundary. In the refinement process, the number of nodes has been increased only in the normal direction and in the C-cut. The main parameters of the four grid levels are provided in Table 4. The analysis has been carried out for $\alpha=4.02^o$ using the K-ε ASM model. The lift and drag coefficient computed with these grids are reported in Table 5. We see that the variation of lift and drag coefficients decreases as the grid is refined, and it takes a value of about 0.2 % for both lift and drag moving from level 3 to level 4. Thus the solution of level 3 can be taken as grid-independent for engineering applications.

Table 4 Grid-defining parameters of 4 grid levels used for mesh refinement analyses ($\alpha=4.02^o$).

Lev	J_{MAX}	I_{BC}	I_{MAX}	N_{NODE}
1	129	81	461	59469
2	201	201	701	140901
3	249	249	797	198453
4	301	301	901	271201

Table 5 Force coefficients computed with 4 refinement levels for $\alpha=4.02^o$.

	L1 - 03	L2 - 03	L3 - 03	L4 - 03
C_L	0.75306	0.75431	0.75243	0.75200
C_D	0.011509	0.01111	0.01121	0.011183

Figure 20 plots C_p^o at the same location where the wake rake was placed (the abscissas are the same as those of Figure 10), and it shows that refining the grid from level 1 to level 4 has a negligible effect on the wake resolution at this station. Further downstream, however, the same grid refinement has a more significant effect on the wake resolution.

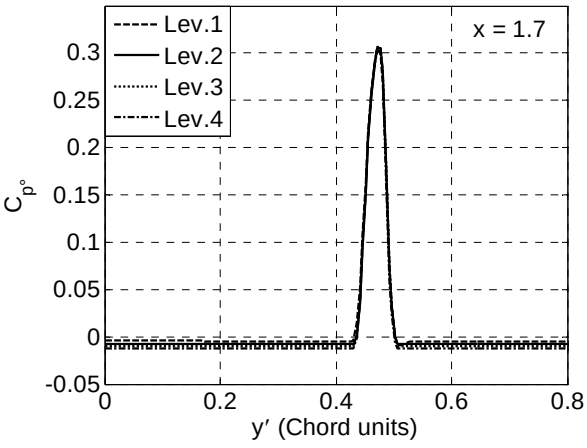

Figure 20 Measured and computed profiles of total pressure coefficient 70 % chord behind TE for $\alpha=4.02^o$. Computed profiles refer to four different refinement levels.

This is highlighted in Figure 21, which reports the profiles of total pressure coefficient 9 chords after the TE along a fictitious wake rake orthogonal to the freestream direction.

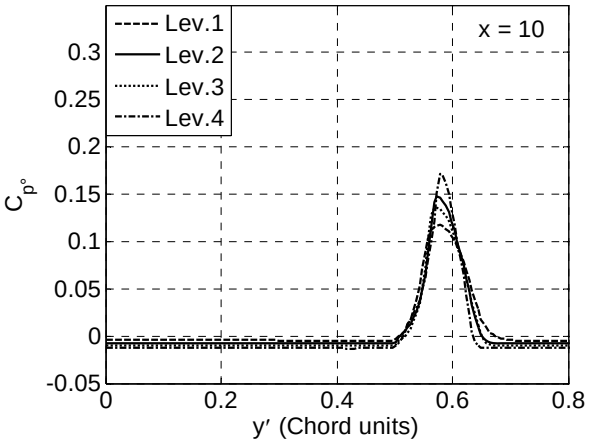

Figure 21 Computed profiles of total pressure coefficient 9 chord behind TE for $\alpha=4.02^o$. Results refer to four different refinement levels.

CONCLUSIONS

.

This study has presented an *a priori* grid adaptation approach for structured grids aimed at improving the resolution of the wake shed by the TE of WT airfoils. The analyses carried out so far show that it is not sufficient to rotate the C-cut, but one has also to build a wake-tracking C-cut close to the Trailing Edge. The wake-adapted grid has also been found to substantially improve the convergence characteristics of the CFD calculations.

This grid adaptation appears to have a small effect on the predicted airfoil forces based on the integration of pressure force and viscous stress, but it may contribute to support the application of mid-field methods for the calculation of airfoil forces, as these methods rely on the wake status.

The construction of the C-cut is currently based on a preliminary XFOIL analysis, but this dependence may be easily circumvented by hardwiring a panel method in the grid generator to determine the wake trajectory needed for the grid generation process.

Additional grid refinements of the adapted grid further improve the far-field wake resolution, but the improvement is smaller than that achieved by adapting the grid for a given overall number of nodes. The coarsest grid without adaptation selected for this study had already a fairly high number of nodes, and therefore it is possible that the effects of adaptation and refinement may be more substantial when starting from coarser meshes often used in engineering applications.

The comparison of transitional and fully turbulent analyses reveals that the errors on the aerodynamic forces introduced by not accounting for transition are of the order of 10 % for the lift and 50 % for the drag force. The comparative analysis of four turbulence models shows that the best prediction of viscous effects is delivered by the K-ω ASM model.

ACKNOWLEDGMENTS

The authors would like to thank Gaia-Wind Ltd. for ontributing to the realization of this study, and the Risoe National Laboratory for providing the geometry and the experimental data of the FFA-W3-241 airfoil. This research

has been carried out in the framework of a project supported by the Engineering and Physical Sciences Research Council under grant EP/F038542/1.

REFERENCES

1. F. Bertagnolio, N.N. Sorensen, F. Rasmussen, New insight into the flow around a wind turbine airfoil section, *Solar Energy Engineering*, vol. 127, pp. 214-222, 2005.

2. C.P. Stone, S.M. Tebo, C.P.N. Duque, Fluid dynamics of flatback airfoils for wind turbine applications, AIAA paper AIAA-2006-194, 2006.

3. A. Le Pape and J. Lecanu, 3D Navier-Stokes computations of a stall-regulated wind turbine, *Wind Energy*, vol. 7, pp. 309-324,2004.

4. R.B. Langtry, J. Gola, F.R. Menter, Predicting 2D airfoil and 3D wind turbine rotor performance using a transitional model for general CFD codes, AIAA paper AIAA-2006-395, 2006.

5. W.P. Wolfe and S.S. Ochs, CFD calculations of S809 aerodynamic characteristics, AIAA paper AIAA-07-0973, 1997.

6. D.C. Wilcox, Reassessment of the scale-determining equation for advanced turbulence models, *AIAA Journal*, vol. 26, pp. 1299-1310, 1988..

7. F.R. Menter, Two-equation eddy-viscosity turbulence models for engineering applications, *AIAA Journal*, vol.32, pp. 1598-1605, 1994.

8. A. Paperone and R. Tognaccini, Computational fluid dynamics-based drag prediction and decomposition, *AIAA Journal*, vol.41, pp. 1647-1657, 2003.

9. P. Fuglsang, I. Antoniou, K.S. Dahl, H,A, Madsen, Wind tunnel tests of the FFA-W3-241, FFA-W3-301 and NACA-63-430 airfoils, Technical Report R-1041(EN), Riso National Laboratory, Denmark, 1998.

10. F. Fraysse and M.S. Campobasso, On the development of flexible multi-block grid generators for the CFD analysis of wind turbine airfoils, Technical report 0706, Department of Aerospace Engineering, University of Glasgow, United Kingdom, 2007.

11. M. Foerster and M.S. Campobasso, Development of a hyperbolic grid generation code and viscous CFD analysis of wind turbine airfoils, Technical report 0802, Department of Aerospace Engineering, University of Glasgow, United Kingdom, 2008.

12. O. Guerri, K. Bouhadef, A. Harhd, Turbulent flow simulation of the NREL S809 airfoil, *Wind Engineering*, vol. 30, pp. 287-302, 2006.

13. J.H. Morrison, A compressible Navier-Stokes solver with two-equation and Reynolds stress turbulence closure models, NASA CR4440, 1992.

14. H.S. Zhang, R.M.C. So, T.B. Gatski, C.G. Speziale, A near-wall second-order scheme for compressible turbulent flows, Near-wall turbulent flows, edited by R.M.C. So, C.G. Speziale, B.R. Launder, Elsevier Science Publishers, B.V. 1933.

15.. T. Gatski, and C. Speziale, On explicit algebraic stress nodels to compute turbulent flows, *Journal of Fluid Mechanics*, vol. 254, pp. 59-78, 1993.

SOMMARIO

Il presente lavoro documenta l'attività di ricerca attualmente condotta presso l'Università di Glasgow riguardante lo studio aerodinamico di rotori eolici. In particolare, vengono messi in evidenza diversi aspetti inerenti la simulazione del campo di moto basata sulla soluzione numerica delle equazioni di Navier-Stokes mediate a la Reynolds (RANS).

Il primo tra questi aspetti riguarda gli effetti di una tecnica di generazione ed infittimento *a priori* di griglie strutturate, volta a migliorare la risoluzione della scia. I risultati presentati mostrano come la strategia proposta consenta di migliorare notevolmente la risoluzione della scia a valle del rotore, laddove questa risulta quasi completamente dissipata dalla viscosità numerica qualora si utilizzino griglie non adattative. La metodologia proposta può essere applicata con facilità a pacchetti software già esistenti per la generazione di griglie strutturate.

Il secondo aspetto riguarda la valutazione degli effetti della modellizzazione numerica della transizione del flusso da laminare a turbolento. Si è osservato, infatti, che i coefficienti di resistenza calcolati considerando il flusso transizionale oppure completamente turbolento differiscono finanche del 50%.

Infine, sono state valutate le caratteristiche previsionali di differenti modelli di turbolenza, confrontando i coefficienti aerodinamici calcolati dai vari modelli.

Questi tre aspetti sono stati studiati utilizzando un generatore di griglie strutturate di tipo iperbolico appositamente sviluppato ed un codice di simulazione ai volumi finiti di tipo multi-blocco. Le simulazioni numeriche sono state condotte per un tipico profilo di rotore eolico per il quale è disponibile un'ampia gamma di dati sperimentali in condizioni di flusso stazionario ed in-stazionario. Le potenzialità del codice di simulazione fluidodinamica sono state valutate confrontando i risultati numerici ed i dati sperimentali per due configurazioni di flusso a diversa incidenza. I risultati ottenuti mediante la simulazione RANS sono inoltre stati confrontati con quelli ottenuti mediante il codice di simulazione XFOIL, basato sul metodo dei pannelli ed un modello di interazione fra strato limite e campo potenziale.